Title	High-resolution scanning electron microscopy for the analysis of three-dimensional ultrastructure of clots in acute ischemic stroke
Author(s)	Mereuta, Oana Madalina; Fitzgerald, Seán; Christensen, Trace A.; Jaspersen, Adam L.; Dai, Daying; Abbasi, Mehdi; Puttappa, Tejaswini; Kadirvel, Ram; Kallmes, David F.; Doyle, Karen M.; Brinjikji, Waleed
Publication Date	2020-12-23
Publication Information	Mereuta, Oana Madalina, Fitzgerald, Seán, Christensen, Trace A., Jaspersen, Adam L., Dai, Daying, Abbasi, Mehdi, Puttappa, Tejaswini, Kadirvel, Ram, Kallmes, David F., Doyle, Karen M., Brinjikji, Waleed. (2020). High-resolution scanning electron microscopy for the analysis of three-dimensional ultrastructure of clots in acute ischemic stroke. Journal of NeuroInterventional Surgery, neurintsurg-2020-016709. doi:10.1136/neurintsurg-2020-016709
Publisher	BMJ Publishing Group
Link to publisher's version	http://dx.doi.org/10.1136/neurintsurg-2020-016709
Item record	http://hdl.handle.net/10379/16649
DOI	http://dx.doi.org/10.1136/neurintsurg-2020-016709

Manuscript Title: High-resolution scanning electron microscopy for the analysis of 3D ultrastructure of clots in acute ischemic stroke

Figures 3, Table 1

Keywords: ischemic stroke, emboli, SBFSEM, composition

Abstract

Background:

Characterization of acute ischemic stroke (AIS) clots has typically focused on two dimensional histological analysis of the thrombus. The three dimensional (3D) architecture and distribution of components within emboli have not been fully investigated.

The aim of this study was to examine the composition and microstructure of AIS clots using histology and serial block-face scanning electron microscopy (SBFSEM).

Methods:

As part of the multi-institutional STRIP registry, ten consecutive AIS emboli were collected from ten patients treated by mechanical thrombectomy. Histological and immunohistochemical analysis was performed to determine clot composition. SBFSEM was used to assess ultrastructural organization of clots and specific features of individual components.

Results:

Quantification of Martius Scarlett Blue stain identified fibrin (44.4%) and red blood cells (RBC, 32.6%) as main components. Immunohistochemistry showed a mean platelet and von Willebrand content of 23.9% and 11.8%, respectively.

The 3D organization of emboli varied greatly depending on the region analyzed. RBC-rich areas were composed of tightly packed RBC deformed into polyhedrocytes with scant fibrin fibers interwoven between cells. Regions with mixed composition showed thick fibrin fibers along with platelets, white blood cells and RBC clusters. Fibrin-rich areas contained dense fibrin masses with sparse RBC. In three cases, the fibrin formed a grid-like or a sponge-like pattern likely due to thrombolytic treatment. Segmentation showed that fibrin fibers were thinner and less densely packed in these cases.

Conclusions:

3D-SEM provides novel and potentially clinically relevant information on clot components and ultrastructure which may help to inform thrombolytic treatment and medical device design.

INTRODUCTION

Histological stains and immunohistochemistry have been widely used to analyze basic composition of acute ischemic stroke (AIS) clots.[1-3] Although these techniques provide valuable data, additional knowledge of the ultrastructural organization of clots may be useful to improve the effectiveness of thrombolysis and mechanical thrombectomy. Serial block-face scanning electron microscopy (SBFSEM) utilizes an 'in chamber' microtome and backscatter detection to scan the block surface of a resin embedded tissue while sectioning. The resulting stack of aligned high resolution images allows for volume renderings that reveal ultrastructural details and 3-dimensional nuances that simply cannot be observed using routine histological approaches. Further segmentation of individual structures within the tissue can provide precise qualitative and quantitative volumetric data.

Standard scanning electron microscopy (SEM) has been used to examine the ultrastructural characteristics of blood clots related to hypo- and hypercoagulable states.[4] It has been shown also that an altered red blood cell, platelet and fibrin network ultrastructure is present in the blood of stroke patients.[5, 6] Furthermore, differences have been found between arterial and venous thrombi and pulmonary emboli that may have implications on the treatment of thrombotic disorders.[7] The 3-dimensional (3D) ultrastructure of AIS emboli, however, has been less characterized.

The objective of our study was to investigate the 3D microstructure of AIS emboli and to identify ultrastructural features of individual components using SBFSEM and 3D imaging in addition to the characterization of clot composition by standard histological analysis.

MATERIALS AND METHODS

Clots collection

This study was performed as part of the multi-institutional Stroke Thromboembolism Registry of Imaging and Pathology (STRIP) registry. The study was approved by the Institutional Review Board and was HIPAA compliant. A waiver of consent was granted. Patients were included in the study if they were >18 years, had undergone mechanical thrombectomy treatment for AIS and had embolic material available for analysis.

We prospectively collected ten consecutive emboli retrieved from ten patients. On retrieval, clots were immediately placed in fresh modified Trumps fixative solution (2% glutaraldehyde + 2% paraformaldehyde in 0.15 M cacodylate buffer containing 2 mM calcium chloride). A representative fragment of each clot was cut transversally or longitudinally in half and gross photos of both fragments were taken (Figures 1A, D). One piece was processed for SBFSEM analysis and the other was processed for histological analysis.

Clot histology and immunohistochemistry

The histological portion of each clot was processed using a standard tissue processing protocol, embedded in paraffin and cut into 3 µm sections. As shown in Figure 2, consecutive slides were stained with Hematoxylin and Eosin (H&E) and Martius Scarlett Blue (MSB) stains to identify the main components.[8] While H&E helps to distinguish between red blood cells (RBC)-rich areas (red/dark pink) and fibrin/platelets-rich areas (light pink), MSB clearly differentiates RBC (yellow), fibrin (red) and platelets/other (light pink) areas.

Immunostaining was used to identify platelets (rabbit monoclonal anti-CD42b, Abcam ab227669) and von Willebrand Factor (monoclonal mouse anti-human vWF, Dako M0616).

Immunohistochemistry was performed on a Leica Bond Max Autostainer using a RedMap kit (Bond Polymer Refine Red Detection, Leica Biosystems).

Stained slides underwent whole slide scanning (Motic Easyscan Pro, Motic Digital Pathology) at 20x magnification. MSB and IHC quantification of clot components was performed using Orbit Image Analysis software (www.orbit.bio) as previously described.[9]

Serial block-face scanning electron microscopy of clots

Fixation and staining

The portion of each clot selected for SBFSEM was processed using a protocol adapted from that published by Hua et al.[10] Briefly, samples were fixed for a minimum of 24 hours, washed in 0.15 M cacodylate buffer and incubated at room temperature in 2% osmium tetroxide in 0.15 M cacodylate for 1.5 hour. Without rinsing, samples were incubated in 2.5% potassium ferracyanide in 0.15 M cacodylate for another 1.5 hour at room temperature. Following a rinse in nH_2O, samples were incubated in 1% thiocarbohydrazide in H_2O for 45 min at 50˚C. After another rinse in nH_2O, samples were incubated sequentially in 2% osmium tetroxide in H_2O for 1.5 hour at room temperature, 1% aqueous uranyl acetate overnight at 4˚C, and 7% lead aspartate solution 1 hour at 50˚C, with several rinses in nH_2O between each reagent. Following dehydration through a series of ethanol and acetone, samples were infiltrated and eventually embedded in epoxy resin Durcapan (EMS, Hatfield, PA) and polymerized in a 60˚C oven for a minimum of 24 hours.

Preparation of embedded samples for imaging

To prepare embedded samples for placement into the SEM and subsequent imaging, 1 mm^3 pieces were roughly trimmed of any excess resin and mounted to 8 mm aluminum stubs using silver epoxy Epo-Tek (EMS, Hatfield, PA). The mounted sample was then carefully trimmed to a 0.5 mm x 0.5 mm x 1 mm tall tower using a diamond trimming knife (Diatome trimtool 45, EMS,

Hatfield, PA). Trimmed sample and entire stub was coated with gold palladium to assist in charge dissipation. The coated sample was then inserted into a VolumeScope serial block-face SEM (Thermo Fisher, Waltham, MA) for imaging.

Acquisition and post-processing of images

Three areas of interest from each sample were selected for serial imaging. High-resolution block-face images were obtained in a low vacuum environment using a beam energy of 3.0 kV with a current of 100 pA, a scanning dwell time of 2 µs and a 10 nm pixel size. A stack of approximately 500 images were obtained while cutting the block at 50 nm increments. The image stack was then aligned, filtered and 3D renderings were created using both *Amira* software (Thermo Fisher, Waltham, MA) and Reconstruct software.[11]

RESULTS

Patient data

Ten consecutive patients diagnosed with AIS were included in the study. There were 5 men and 5 women. The mean age was 69 years (range 54-81 years). Suspected stroke etiologies were cardioembolic (6 cases), Large Artery Atherosclerosis (2 cases), unknown etiology (1 case) and other suspected etiology (1 case). Two patients had an occlusion of the internal carotid artery. Middle cerebral artery (M1) was occluded in 6 patients and basilar artery in 2 cases. The clots were extracted at first attempt in 6 cases. Multiple procedural passes were required in 4 cases. Successful recanalization (final mTICI 2b/3) was achieved in all cases. Aspiration was used in 7 cases. A combined approach of stentriever and aspiration device was used in 3 patients. Three patients were treated with recombinant tissue plasminogen activator (rt-PA) as follows: Case 2-intravenous (Alteplase IV bolus and infusion) and intraarterial administration; Case 7-only intravenous (Alteplase IV bolus); Case 10-only intravenous (Alteplase IV bolus and infusion).

The main characteristics of patients are summarized in Table 1.

Table 1. Occlusion information and interventional details of study cases.

Case #	rt-PA treatment	Stroke etiology	Site of Occlusion	Number of Passes	Final mTICI Score	Technique
1	No	Unknown	ICA	1	3	Aspiration
2	Yes	Cardioembolic	Basilar	2	2b	Combination
3	No	Large Artery Atherosclerosis	M1	1	3	Aspiration
4	No	Cardioembolic	ICA	3	2b	Combination
5	No	Other	M1	2	3	Aspiration
6	No	Large Artery Atherosclerosis	Basilar	1	3	Aspiration
7	Yes	Cardioembolic	M1	1	2b	Aspiration
8	No	Cardioembolic	M1	3	3	Aspiration
9	No	Cardioembolic	M1	1	3	Combination
10	Yes	Cardioembolic	M1	1	3	Aspiration

rt-PA: recombinant tissue plasminogen activator; ICA: internal carotid artery; M1: horizontal segment of the middle cerebral artery; mTICI Score: modified Thrombolysis in Cerebral Infarction Score.

Histological composition of thrombi

H&E and MSB stains identified the major components of clots (Figures 2A, B). We noticed that clots presented two distinct morphological patterns: 1) a RBC-rich core and fibrin/platelet-rich areas distributed toward the periphery (2 cases); 2) RBC-rich and fibrin/platelet-rich areas interspersed with each other (8 cases).

The white blood cells (WBC, blue nuclei) were mainly distributed throughout the fibrin/platelet-rich areas (Supplementary Figure 1A) and were less abundant in the RBC-rich areas (Supplementary Figure 1B). In some emboli, WBC were clustered at the boundary between the RBC-rich and platelet-rich regions (Case 2 and Cases 6-8; Supplementary Figure 1C).

Overall, the clots included in our study had a mixed composition. Quantification of MSB stain showed a mean content of 32.6% RBC (range 1.5%-62.2%), 44.4% fibrin (range 18.6%-78.9%), 19.2% platelets/other (range 1.4%-59.3%) and 3.8% WBC (range 0.3%-8.4%).

Immunostaining for platelets confirmed that platelet/other-rich regions identified by MSB stain were also CD42b and vWF-positive (Figures 2C, D: purple). The mean platelet content was 23.9% and the mean vWF level was 11.8%. As shown in Supplementary Figure 1, platelet-rich areas consisted of islands of platelets surrounded by fibrin (D) and vWF (E) suggesting that the fibrin structures were aligned with vWF.

SBFSEM imaging of thrombi

As shown in Figures 1 and 3, serial block-face imaging and 3D rendering revealed distinct ultrastructural features between clots as well as among different regions within a clot. RBC-rich areas were mainly composed of RBC packed tightly together with a small number of thin fibrin fibers interwoven between the cells (Figures 1B, C and Figures 3A, F). The regions with mixed composition contained bundles of fibrin fibers, platelets, numerous WBC and RBC clusters generating a densely packed matrix (Figures 1E, F and Figures 3B-D; Supplementary Figure 2 and Supplementary File 2). The fibrin-rich regions showed dense fibrin masses and a few RBC trapped in the fibrin mesh (Figures 3E, G).

Unique features of individual components within emboli are also identified. Compressed RBC deformed into polyhedral cells termed polyhedrocytes, likely as a result of clot contraction, were observed in all clots (example shown in Figure 3A, shaded yellow). However, RBC with regular biconcave shape were also present in one case (Figure 3B, shaded yellow). Fibrin formed two different structures that were identified in all clots: thin fibrin strands in the RBC-rich regions

(Figures 1B, C and Figures 3A, F) and thick fibers forming bundles in the fibrin-rich regions (Figures 3E, G) and areas with mixed composition (Figures 1E, F and Figures 3B-D).

Three patients in our cohort received rt-PA treatment. In two cases, in the RBC-rich and mixed regions analyzed, we noticed that fibrin fibers were arranged in a grid-like pattern with polyhedrocytes filling the gaps (Figure 3F-Case 2 and Figure 3D-Case 10). Moreover, segmentation performed in Case 2 showed that fibrin fibers were thinner and less densely packed around the polyhedrocytes compared to a non-rt-PA clot (Figure 3E-Case 3; Supplementary File 3). In another case, the fibrin fibers were evenly distributed but less distinct, with small pieces of fibers missing which created a sponge-like pattern (porous amorphous structure) in the fibrin-rich area analyzed, perhaps as the result of less rt-PA exposure. Segmentation in this case showed that fibrin fibers were similarly thinner and less densely packed (Figure 3G-Case 7; Supplementary File 3).

Platelets were a major component of clots presenting mainly as aggregates attached to fibrin fibers (Figure 3A, blue arrow and shading). We also observed the presence of granular structures along with fibrin strands and WBC which were likely released by platelets during activation and degranulation (Figure 1F, blue arrow; Supplementary Figure 2). WBC were abundantly located within the fibrin-rich and platelet-rich areas and rarely in the RBC-rich regions (Figure 1F and Figures 3A, B, white arrows).

DISCUSSION

In the present study, we characterized the morphological patterns and 3D architecture of AIS emboli using SBFSEM in addition to histological and immunohistochemical analysis. Despite the considerable differences in clot composition revealed by the quantification of specific components and the heterogeneity within the clots, the distribution of RBC-rich and fibrin/platelet-rich regions consisted of two main morphological patterns. We also showed that fibrin/platelets-rich areas are composed of high amounts of fibrin, platelets, vWF and numerous WBC. The 3D volume renderings confirmed the morphological patterns described histologically and identified specific changes of RBC, platelets and fibrin structure within the regions analyzed that cannot be detected by histology. In particular, segmentation of fibrin network revealed major structural changes related to rt-PA treatment.

The SBFSEM analysis indicated in all clots analyzed the presence of RBC-rich areas consisting of polyhedrocytes. This specific change of RBC shape represents a morphological marker of clot contraction which is a common process *in vivo* resulting from compression by activated contractile platelets pulling on fibrin.[12] Comparably, polyhedrocytes do not form when platelet concentrations are low [13] or platelet function is impaired,[14] as this would not generate enough compressive force. Subsequently, platelet-driven contraction would be affected which may explain the absence of RBC shape change in AIS clots like in one of our cases.

Another structural signature of clot contraction previously reported is the redistribution of platelet aggregates and fibrin on the surface of the clot and compression of erythrocytes in the interior of the clot.[15] Contraction pulls clots closer to the vessel wall helping to reduce the obstruction. Therefore, compacted RBC may prevent vascular occlusion but in the same time, may confer resistance to fibrinolysis by reducing clot permeability for thrombolytic enzymes.[16] This

is in agreement with previous studies showing that increased clot perviousness is associated with high levels of RBC within the clots [17] as they may contain less compacted RBC. However, the pathophysiological implication of compacted polyhedrocytes is complex and suggests that RBC content evaluated by histology may not be considered predictive of clot permeability.

The degree of RBC compression may also interfere with mechanical thrombectomy.[12] Different types of clot analogs have been used to evaluate the performance of thrombectomy devices [13] as well as to investigate specific clot behavior such as clot indentation/integration.[18] A recent study showed that the depth of single strut indentation and the degree of clot integration into device during an embedding time of 5 mins correlated with the RBC content of the clot.[18] On the other hand, the extent of clot contraction is hematocrit-dependent as clot analogs corresponding to a lower hematocrit contract more than clots with higher hematocrit. Moreover, platelet-contracted clot analogs are characterized by increased stiffness and their microstructure is different from non-contracted analogs consisting of compacted fibrin around polyhedrocytes.[13] Therefore, platelet-driven contraction and the compaction of polyhedrocytes may affect the mechanical behavior of clots during thrombectomy.

The presence of WBC mainly in the fibrin-rich and platelet-rich regions and occasionally at the interface between the RBC-rich and platelet-rich areas represents another interesting aspect of clot structure that has been previously described.[19] Moreover, activated WBC release proteases and oxygen metabolites that affect adjacent cells including RBC which may suffer alterations in the cell membrane.[5] When exposed to an oxidative and proteolytic environment, RBC may suffer physical and/or molecular damage such as a significant increase of membrane bound hemoglobin and a different band 3 profile.[20] Since the band 3 links the lipid bilayer to the cytoskeleton, any modification in its profile may lead to the destabilization of membrane

structure and subsequently, may compromise the ability of erythrocyte's cytoskeleton to promote membrane deformation. Finally, this may impact clot contraction and the compactness of thrombi.[12]

Specific fibrin structures were identified by 3D-SEM analysis in areas with different composition. A higher platelet content may contribute to fibrin bundle formation, since platelets pull on fibrin fibers, decreasing the space between them, thereby promoting orientation and association of fibers into bundles.[7] Contracting (activated) platelets have been shown to actively remodel the fibrin network of thrombi creating a dense fibrin mesh and increasing clot stiffness.[21] The compaction of polyhedral RBC and modification of the fibrin network, together with other biological factors, have been previously shown to contribute to the rt-PA resistance.[19, 22, 23]

Interestingly, we described a distinct fibrin organization in three clots (i.e., grid-like and sponge-like patterns) that are likely to be caused by the rt-PA therapy. The fact that we found two different patterns may be explained by the different regions analyzed and also by different exposure to rt-PA between these cases. Our observation that vWF and fibrin are associated and delineate platelet-rich islands is in agreement with a previous study [19] and may account for a different response to thrombolysis in our cases. Nevertheless, the segmentation of fibrin network in the rt-PA-treated clots showed that fibrin fibers were thinner and less densely packed compared to non-treated clots. Taken together, these findings are relevant and may help to better understand the rt-PA mechanism of action and how it can affect the 3D microstructure of clots. However, further studies on larger cohorts are required to confirm our hypothesis.

Structural characterization of AIS clots typically involves the use of histology with possibly standard transmission or scanning electron microscopy. These techniques are limited to

2-dimensional observations and minimal volume analysis through the clot. SBFSEM provides a vastly expanded view and allows to study the 3D architecture and distribution of clot components in a manner that has not been possible in the past. The use of this innovative technique may be implemented as a new protocol for thrombus collection and analysis similar to the protocol described in a previous study aimed to investigate the gene expression and proteomic profile of clots and surrounding intraluminal blood.[24]

Our study has limitations related to the low number of emboli analyzed, the potential effect of chemical and physical manipulation on the internal organization of clots, sampling variability, a somewhat subjective evaluation and the lack of a quantitative SEM approach that would add in-depth knowledge on the structural changes described here.

In conclusion, this study demonstrates that the analysis of 3D ultrastructure of AIS emboli complements the histological assessment of clot composition and highlights how the interaction between clot components may influence the structural and mechanical properties of the clot. The 3D-scanning electron microscopy has been shown to be a highly sensitive ultrastructural technique that can detect specific changes of clot organization and individual components which may advance the understanding of sub-cellular alterations related to clot formation and ultimately improve the treatment of AIS patients.

REFERENCES

1. De Meyer SF, Andersson T, Baxter B, et al. Analyses of thrombi in acute ischemic stroke: A consensus statement on current knowledge and future directions. *Int J Stroke* 2017;12:606-14.

2. Brinjikji W, Duffy S, Burrows A, et al. Correlation of imaging and histopathology of thrombi in acute ischemic stroke with etiology and outcome: a systematic review. *J Neurointerv Surg* 2017;9:529–34.

3. Fitzgerald S, Mereuta OM, Doyle KM, et al. Correlation of imaging and histopathology of thrombi in acute ischemic stroke with etiology and outcome. *J Neurosurg Sci* 2019;63:292-300.

4. Pretorius E, Swanepoel AC, DeVilliers s, et al. Blood clot parameters: thromboelastography and scanning electron microscopy in research and clinical practice. *Thromb Res* 2017;154:59-63.

5. Swanepoel AC, Pretorius E. Scanning electron microscopy analysis of erythrocytes in thromboembolic ischemic stroke. *Int J Lab Hematol* 2012;34:185-91.

6. Lipinski B, Pretorius E, Oberholzer HM, et al. Iron enhances generation of fibrin fibers in human blood: implications for pathogenesis of stroke. *Microsc Res Tech* 2012;75:1185-90.

7. Chernysh IN, Chandrasekaran N, Kosolapova S, et al. The distinctive structure and composition of arterial and venous thrombi and pulmonary emboli. *Sci Rep* 2020;10:5112.

8. Fitzgerald ST, Wang S, Dai D, et al. Platelet-rich clots as identified by Martius Scarlett Blue staining are isodense on NCCT. *J Neurointerv Surg* 2019;11:1145-49.

9. Fitzgerald S, Wang S, Dai D, et al. Orbit image analysis machine learning software can be used for the histological quantification of acute ischemic stroke blood clots. *PLoS One* 2019;14:e0225841. doi: 10.1371/journal.pone.0225841.

10. Hua Y, Laserstein P, Helmstaedter M. Large-volume *en-bloc* staining for electron microscopy-based connectomics. *Nat Commun* 2015;6:7923.

11. Fiala JC. Reconstruct: a free editor for serial section microscopy. *J Microsc* 2005;218:52-61.

12. Tutwiller V, Mukhitov AR, Peshkova AD, et al. Shape changes of erythrocytes during blood clot contraction and the structure of polyhedrocytes. *Sci Rep* 2018;8:17907.

13. Johnson S, Chueh J, Gounis MJ, et al. Mechanical behavior of in vitro blood clots and the implications for acute ischemic stroke treatment. *J Neurointerv Surg* 2020;12:853-7.

14. Tutwiler V, Peshkova AD, Andrianova IA, et al. Contraction of blood clots is impaired in acute ischemic stroke. *Arterioscler Thromb Vasc Biol* 2017;37:271–9.

15. Cines DB, Lebedeva T, Nagaswami C, et al. Clot contraction: compression of erythrocytes into tightly packed polyhedral and redistribution of platelets and fibrin. *Blood* 2014;123:1596-1603.

16. Weisel J, Litvinov R. Red blood cells: the forgotten player in hemostasis and thrombosis. *J Thromb Haemost* 2019;17:271-82.

17. Benson JC, Fitzgerald ST, Kadirvel R, et al. Clot permeability and histopathology: is a clot's perviousness on CT imaging correlated with its histologic composition? *J Neurointerv Surg* 2020;12:38-42.

18. Weafer FM, Duffy S, Machado I, et al. Characterization of strut indentation during mechanical thrombectomy in acute ischemic stroke clot analogs. *J Neurointerv Surg* 2019;11:891-7.

19. Staessens S, Denorme F, Francois O, et al. Structural analysis of ischemic stroke thrombi: histological indications for therapy resistance. *Haematologica* 2020;105:498-507.

20. Santos-Silva A, Rebelo I, Castro E, et al. Erythrocyte damage and leukocyte activation in ischemic stroke. *Clin Chim Acta* 2002;320:29-35.

21. Kim OV, Litvinov RI, Alber MS, et al. Quantitative structural mechanobiology of platelet-driven blood clot contraction. *Nat Commun* 2017;8:1274.

22. Di Meglio L, Desilles JP, Ollivier V, et al. Acute ischemic stroke thrombi have an outer shell that impairs fibrinolysis. *Neurology* 2019;93:e1686-e1698. doi: 10.1212/WNL.0000000000008395.

23. Li Y, Wang H, Zhao L, et al. A case report of thrombolysis resistance: thrombus ultrastructure in an ischemis stroke patient. *BMC Neurol* 2020;20:135.

24. Fraser JF, Collier LA, Gorman AA, et al. The Blood And Clot Thrombectomy Registry AND Collaboration (BACTRAC) protocol: novel method for evaluating human stroke. J Neurointerv Surg 2019;11:265-70.

FIGURE LEGENDS

Figure 1. Serial block-face analysis of thrombi in two representative cases. Clots were cut transversally (A) or longitudinally (D) in half with one piece processed for histopathological analysis and the other processed for serial block-face scanning electron microscopy (SBFSEM). (A) Gross examination of a transversally cut clot (Case 4) shows the presence of a red blood cell (RBC)-rich core (yellow arrow) and a fibrin/platelet-rich areas distributed mainly toward the periphery (red arrow). (B) Volume rendering of the RBC-rich core assembled from serial block-face imaging highlights the tightly packed arrays of polyhedral erythrocytes (polyhedrocytes, yellow arrow) intermixed with a limited volume of thin fibrin fibers (red arrow). (D) Gross examination of a longitudinally cut clot (Case 8) shows RBC-rich regions (yellow arrow) and fibrin/platelet-rich regions (red arrows) interspersed within the clot. (E) SBFSEM volume rendering highlights a region with mixed composition, consisting of both polyhedrocytes (yellow arrow) and dense network of fibrin fibers (red arrow). (C, F) A representative single 2D image from each volume used to generate the 3D rendering shows the different composition of each clot (yellow arrows=RBC, red arrows=fibrin). Note the presence of numerous white blood cells (white arrows) and granules likely released by platelets (blue arrow) within a densely packed fibrin network. Scale bar = 10 μm.

Figure 2. Histological and immunohistochemical analysis of thrombi included in the study. Consecutive sections were stained with: (A) Hematoxylin and Eosin (H&E), (B) Martius Scarlett Blue (MSB), (C) anti-CD42b (platelets) and (D) anti-von Willebrand factor (vWF) antibodies. H&E shows red blood cells (RBC)-rich areas (red/dark pink) and fibrin/platelets-rich areas (light pink). MSB identifies the main components: RBC (yellow), fibrin (red), platelets/other (light pink) and white blood cells (WBC, blue nuclei). Two distinct morphological patterns were present: 1)

an RBC-rich core and fibrin/platelet-rich areas distributed toward the periphery (Case 1 and Case 4); 2) RBC-rich and fibrin/platelet-rich areas interspersed with each other (Case 2, Case 3 and Cases 5-10). WBC were mainly distributed throughout the fibrin-rich and platelet-rich areas. Platelet/other-rich regions identified by MSB stain (B) were also positive (purple) for CD42b (C) and vWF (D). Scale bar = 3 mm (Case 1 and Case 2) and 2 mm (Cases 3-10).

Figure 3. Detailed ultrastructural organization and characteristics of individual thrombi components observed using serial block-face imaging. (A) Clot area with densely packed red blood cells (RBC) as polyhedrocytes (shaded yellow) and rare white blood cells (WBC, white arrow). Platelet aggregates are attached to fibrin fibers (blue arrow and shading). (B) Clot area with mixed composition showing standard shaped biconcave erythrocytes (shaded yellow) and also polyhedrocytes (bottom of image). Note the presence of numerous WBC (white arrows). (C, D) Clots with mixed composition containing densely packed polyhedrocytes and dense fibrin patches in Case 5 compared to Case 10 showing a grid-like pattern of fibrin network and less compacted polyhedrocytes likely due to recombinant tissue plasminogen activator (rt-PA) treatment in this case. (E-G) Comparison of clots with and without rt-PA treatment. The 3D model in the far right panel for each case represents the area marked in the middle panel (white box). (E) Fibrin-rich area of an untreated clot (Case 3) with thick fibrin fibers that are densely packed. (F) rt-PA treated clot (Case 2) showing a grid-like pattern of fibrin. Segmentation demonstrates that fibrin fibers are loosely packed and thinner. (G) rt-PA treated clot (Case 7) consisting of a sponge-like pattern of fibrin (porous amorphous structure) and a few RBC. The fibrin in this clot is also thinner and less densely packed. Scale bar = 10 μm (A-D) and 5 μm (E-G).

SUPPLEMENTARY MATERIAL

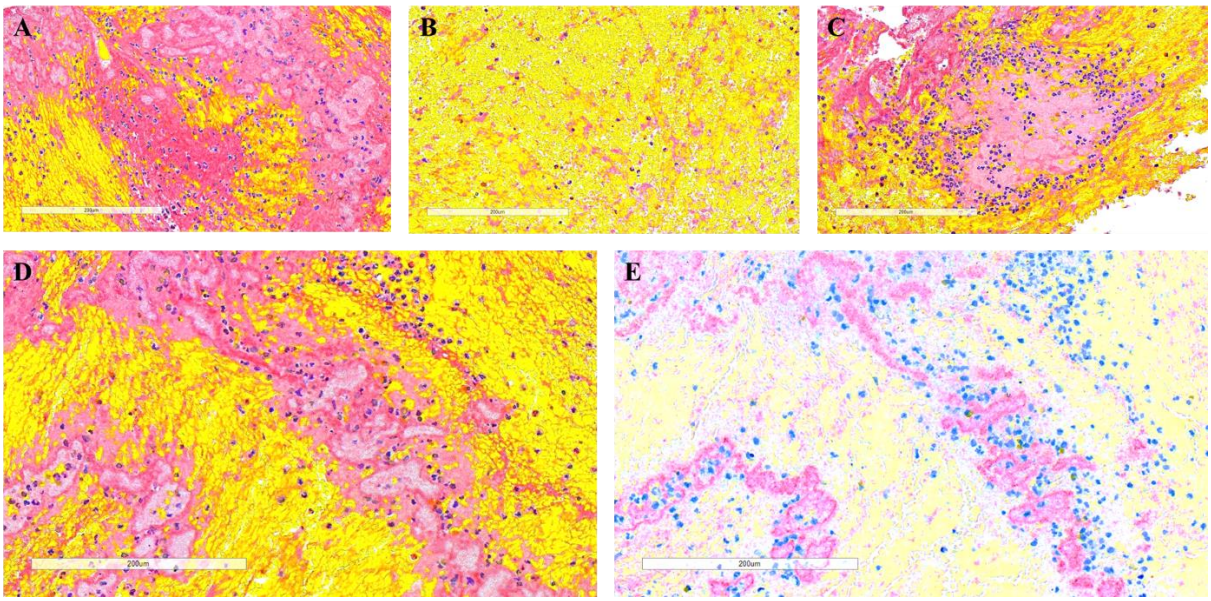

Supplementary Figure 1. Morphologial features of thrombi in a representative case.

(A-D) Martius Scarlett Blue (MSB) staining in Case 2 demonstrates the presence of red blood cells (RBC, yellow), white blood cells (WBC, blue nuclei), fibrin (red) and platelets/other (light pink). WBC are predominantly distributed within the fibrin/platelet-rich areas (A) and are less abundant in the RBC-rich areas (B). WBC can be also located at the boundary between RBC-rich and platelet/fibrin-rich regions. (D) MSB showing islands of platelets surrounded by fibrin. (E) von Willebrand Factor (vWF) immunohistochemistry in the same area shows that the islands of platelets were also surrounded by vWF (purple). Scale bars = 200 µm (A-E).

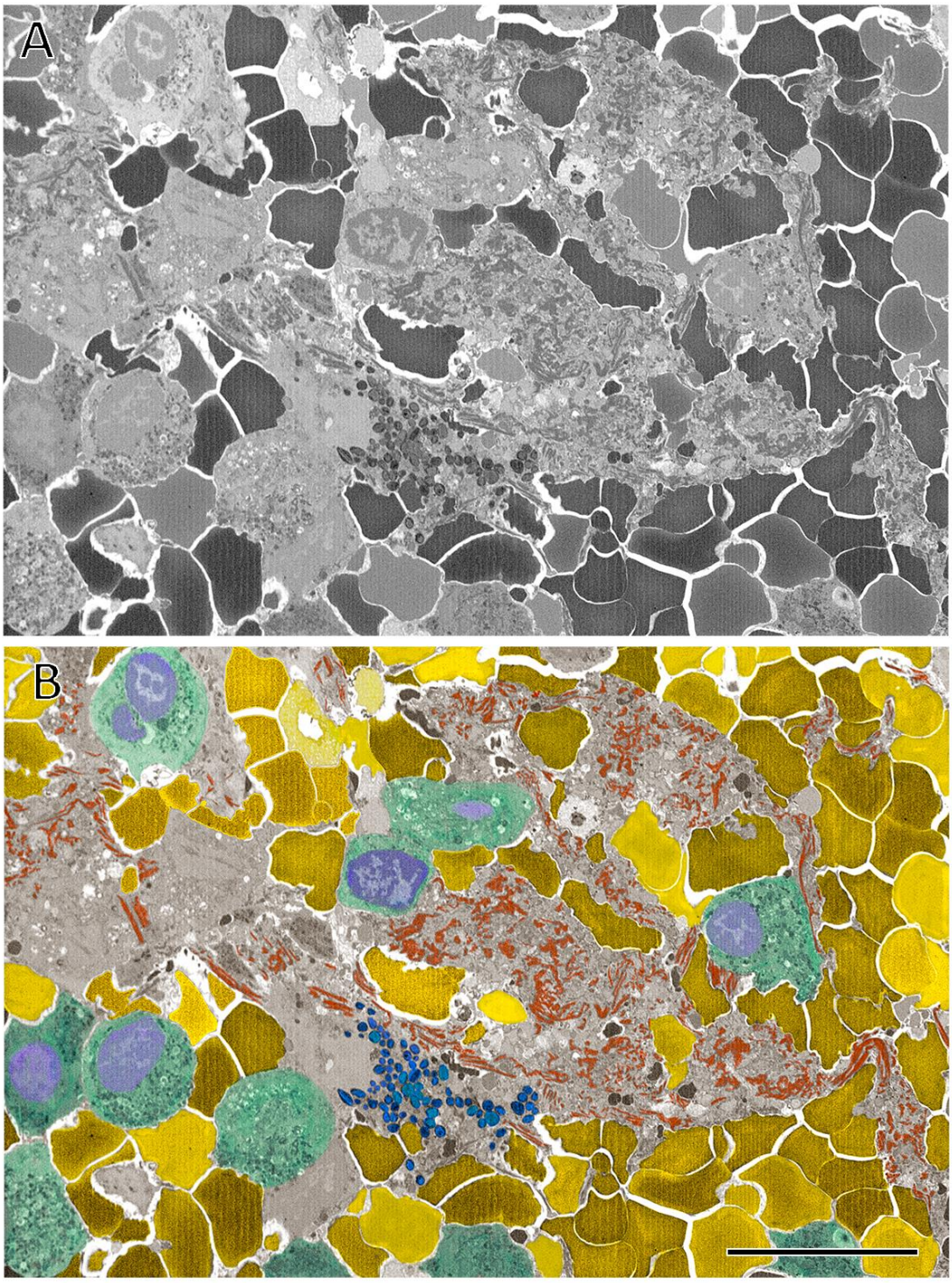

Supplementary Figure 2. Complex microstructure of a representative clot.

(A) Representative original 2D image of the clot from Case 8 showing mixed composition. (B) Colorized version of same image highlighting different components of the clot: fibrin (red), red blood cells (yellow), white blood cells (green), released immune granules (blue). Scale bar = 10 μm.

Supplementary File 2 – Multimedia file

Movie showing 400 consecutive block-face images stacked and aligned from Case 8. 50 nm sections were cut from the block-face between each image. Images are viewed through the z-plane as well as the x-y plane. Note the compressed red blood cells forming polyhedrocytes and the dense fibrin network containing numerous granulated white blood cells and platelets.

Supplementary File 3– Multimedia file

Movie showing 360º rotation of fibrin networks segmented from Cases 3, 2 and 7.

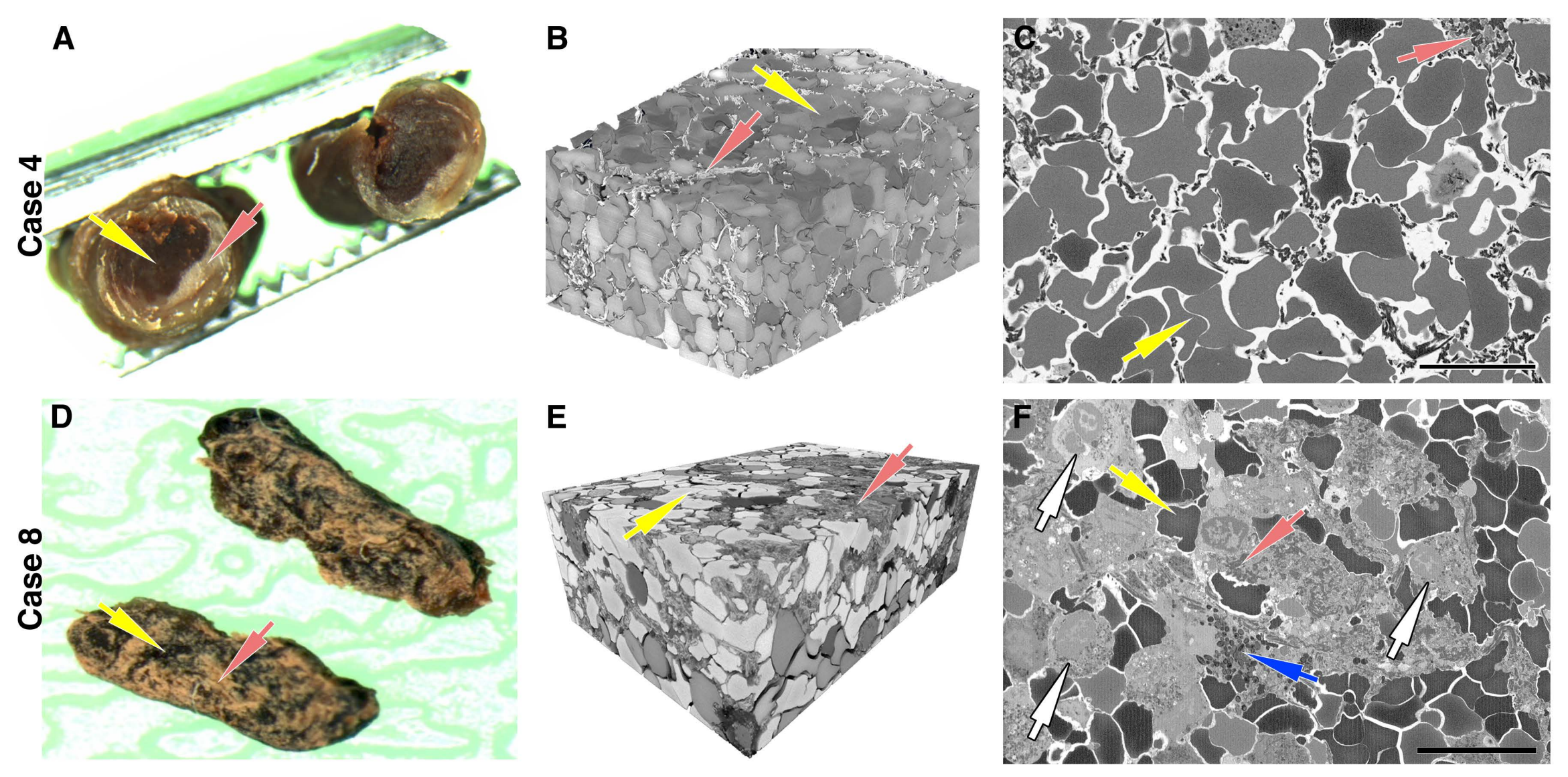
A
B
C
Case 4
D
E
F
Case 8

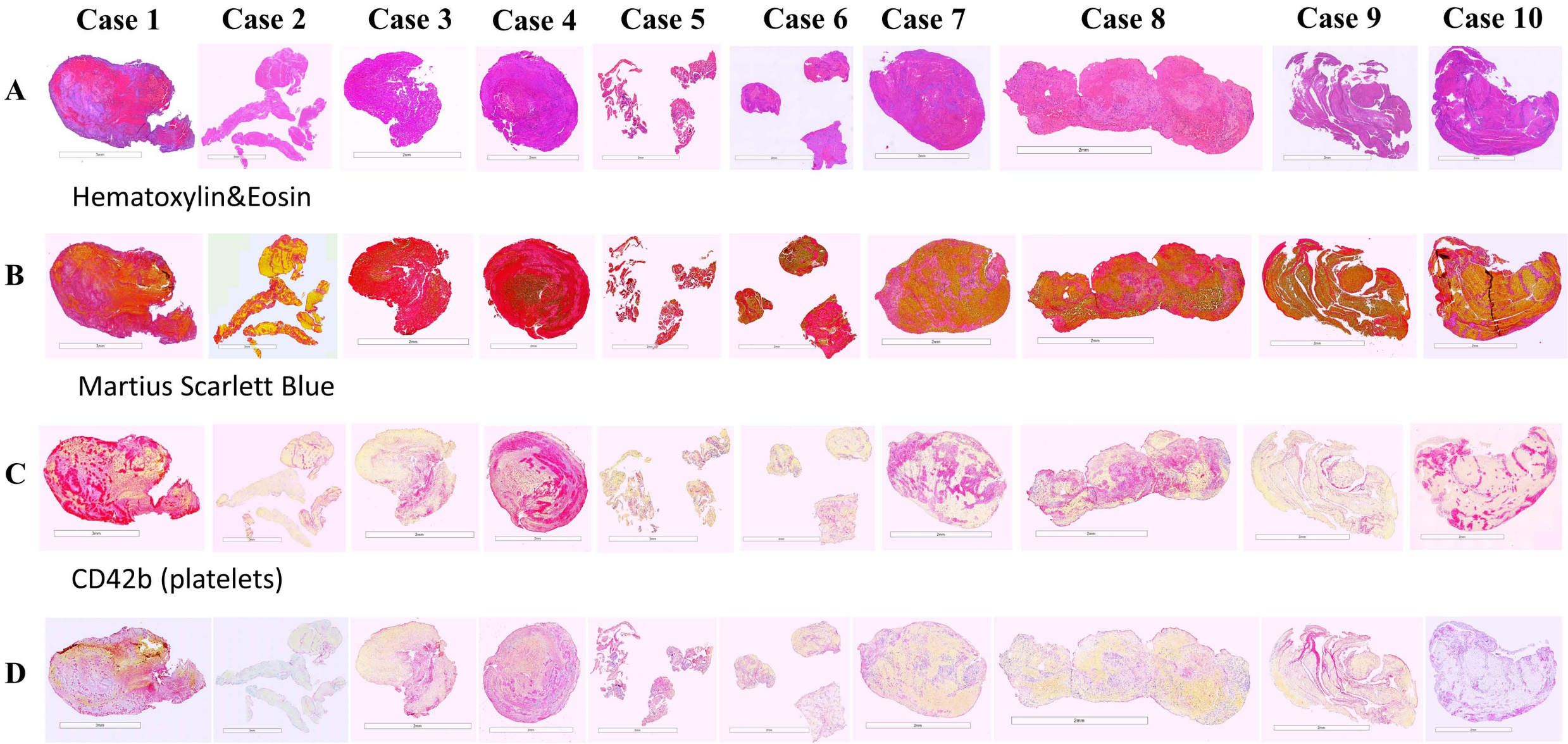
Case 1
Case 2
Case 3
Case 4
Case 5
Case 6
Case 7
Case 8
Case 9
Case 10
A
Hematoxylin&Eosin
B
Martius Scarlett Blue
C
CD42b (platelets)
D
von Willebrand Factor

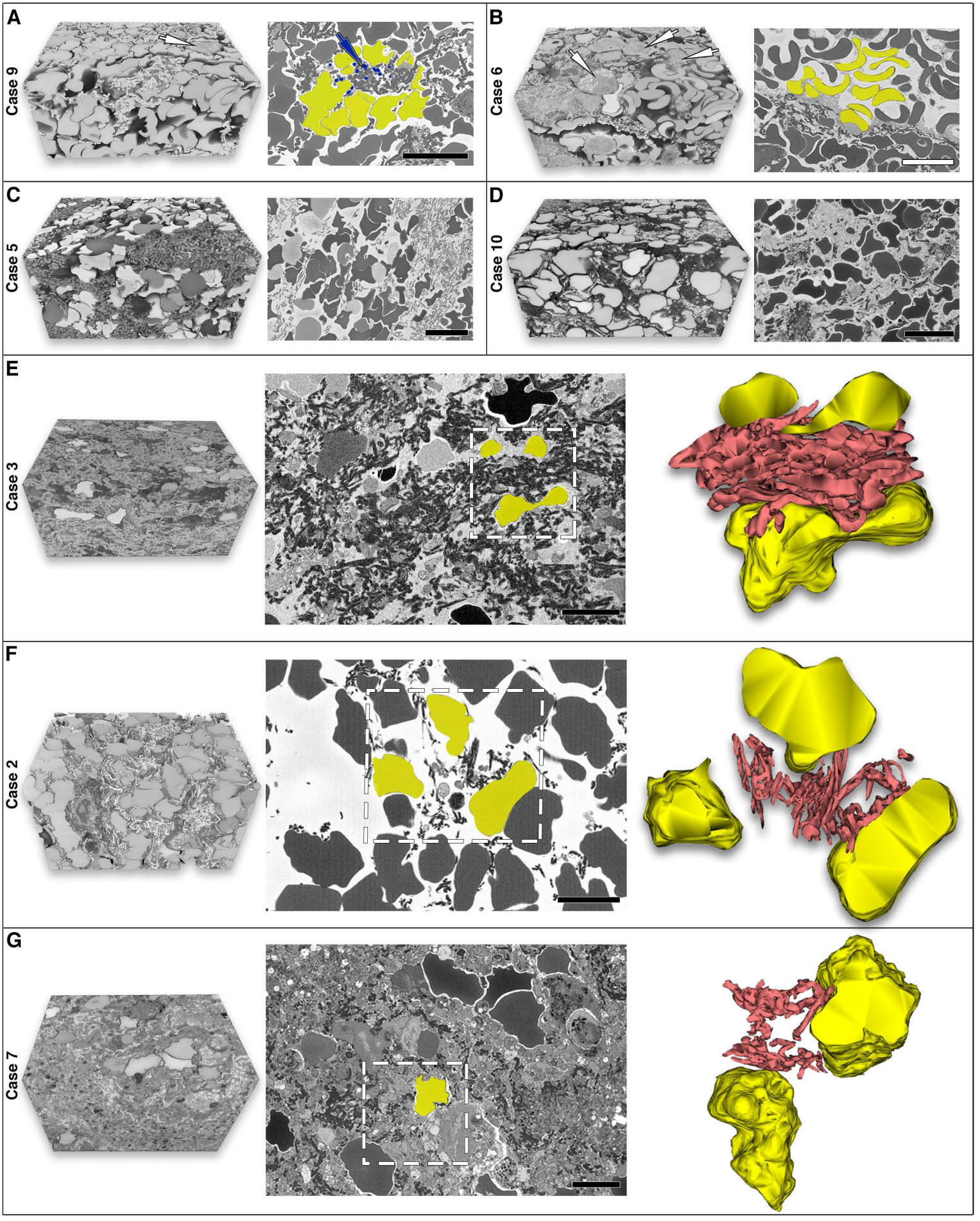
A
Case 9
B
Case 6
C
Case 5
D
Case 10
E
Case 3
F
Case 2
G
Case 7